Interaction of the Low-Affinity Receptor CD23/FcεRII Lectin Domain with the Fcε3−4 Fragment of Human Immunoglobulin E†

Jianguo Shi,‡ Rodolfo Ghirlando,§,|| Rebecca L. Beavil,‡ Andrew J. Beavil,‡ Maura B. Keown,‡ Robert J. Young,‡,⊥ Raymond J. Owens,▽ Brian J. Sutton,‡ and Hannah J. Gould*,‡

The Randall Institute, King's College London, 26−29 Drury Lane, London WC2B 5RL, United Kingdom, Celltech Therapeutics Ltd., 216 Bath Road, Slough SL1 4EN, United Kingdom, and Laboratory of Molecular Biology, National Institute of Diabetes, Digestive, and Kidney Diseases, National Institutes of Health, Bethesda, Maryland 20892−0540

Received May 23, 1996; Revised Manuscript Received November 4, 1996⊗

ABSTRACT: CD23/FcεRII, the low-affinity receptor for IgE, is a multifunctional protein of importance in blood cell development and the immune system. We have studied the interaction of CD23 with IgE in solution using hydrodynamic methods applied to recombinant fragments of both ligands: sCD23, corresponding to the soluble lectin domain of CD23, and Fcε3−4, a dimer of the Cε3−Cε4 sequence of IgE. The hydrodynamic, spectroscopic, and biological properties of these fragments suggest that they have a fully native structure. Sedimentation equilibrium studies on mixtures of sCD23 and Fcε3−4 indicate that IgE has two binding sites for CD23, each characterized by affinities of approximately 10^5 M^{-1}. Analysis of the sedimentation as a function of temperature allows conclusions to be drawn about the thermodynamics of binding at the two sites. Binding at the first site is characterized by large changes in enthalpy ($\Delta H°_{T_o} = -2.1 \pm 3.3$ kcal mol^{-1}) and heat capacity ($\Delta Cp° = -320 \pm 320$ cal mol^{-1} K^{-1}), whereas binding at the second site is characterized by small changes in enthalpy ($\Delta H°_{T_o} = 0.1 \pm 5.6$ kcal mol^{-1}) and heat capacity ($\Delta Cp° = -140 \pm 550$ cal mol^{-1} K^{-1}). In native CD23, there are two or three lectin domains, associated through an α-helical coiled-coil stalk. The predicted structure of the CD23 oligomers and symmetry considerations rule out the possibility of two lectin domains from one oligomer binding to identical sites in IgE. The notion of two types of interaction in the 2:1 complex between CD23 and IgE is consistent with the thermodynamic data presented.

CD23[1] or FcεRII is the low-affinity receptor for IgE and mediates the effector functions of IgE in antigen presentation (Kehry & Yamashita, 1989; Pirron et al., 1990; Heyman et al., 1993; Gustavsson et al., 1994), cytotoxic cell activity (Yokota et al., 1992), and the feedback regulation of IgE synthesis (Sutton & Gould, 1993). Though it is called the "low-affinity" IgE receptor, it actually binds to IgE with fairly high affinity ($K_a = 6.3 \times 10^7$ M^{-1}) (Spiegelberg, 1984) compared to that of the interaction of IgG receptors with IgG (ranging from 10^6 to 10^8 M^{-1}) (Ravetch & Kinet, 1991); the name stems from the fact that the affinity of CD23 for IgE is low relative to that of the "high-affinity" IgE receptor, FcεRI ($K_a = 10^{10}$ M^{-1}). The CD23−IgE interaction is less well characterized than the FcεRI−IgE interaction.

Unlike the other Fc receptors, including FcεRI, which are members of the Ig superfamily, CD23 is a C-type lectin and a type II integral membrane protein (having an extracellular C-terminal sequence and an intracellular N-terminal sequence). The lectin domain lies in the extracellular sequence near the C terminus and is separated from the membrane by a sequence of about 100 amino acids that forms a two- or three-stranded, 10 nm-long α-helical coiled-coil stalk (Beavil et al., 1992). Formation of this structure results in the oligomerization of the lectin domains. Endogenous proteases cleave CD23, initially at the base of the stalk to release oligomeric fragments. Subsequent proteolytic cleavage reduces the fragments to 25 kDa and then to 16 kDa monomers; the latter contains only the lectin domain and still binds to IgE, but with lower affinity than native CD23 (Bettler et al., 1989; this work). CD23 fragments are implicated in a variety of important biological activities [reviewed in Delespesse et al. (1991) and Sutton and Gould (1993)]. In particular, the 16 kDa fragment exhibits suppressive activity in the stimulation of IgE synthesis by IL-4 plus hydrocortisone *in vitro* (Sarfati et al., 1992). These fragments are thought to exert their activities in a paracrine fashion as they are released from the surface of cells *in situ* (Gordon et al., 1989, 1991).

† Supported by a Collaborative Award in Science and Engineering Studentship to M.B.K., a Wellcome Trust programme grant, and a National Asthma Campaign (U.K.) project grant to B.J.S. and H.J.G. R.G. acknowledges a British Council (France) short visit grant.

* Author to whom correspondence should be addressed at The Randall Institute, King's College London, 26−29 Drury Lane, London WC2B 5RL, United Kingdom. Telephone: 011-44-171-465-5355. Fax: 011-44-171-497-9078.

‡ King's College London.

§ National Institutes of Health.

|| Present address: Centre de Biochimie Structurale, Faculté de Pharmacie, CNRS UMR 9955-UM 1-INSERM U 414, 15 Avenue Charles Flahault, 34060 Montpellier Cedex, France.

⊥ Present address: MRC Laboratory of Molecular Biology, Hills Road, Cambridge CB2 2QH, United Kingdom.

▽ Celltech Therapeutics Ltd.

⊗ Abstract published in *Advance ACS Abstracts,* February 1, 1997.

[1] Abbreviations: Ig, immunoglobulin; Fc, C-terminal fragment of Igs responsible for effector functions; FcγR, IgG receptors; FcεRI, high-affinity IgE receptor; FcεRII or CD23, low-affinity IgE receptor; sFcεRIα, soluble fragment of the FcεRI α-chain; Cε2, Cε3, and Cε4, IgE ε-heavy chain constant regions 2−4, respectively; Cγ2 and Cγ3, IgG γ-heavy chain constant regions 2 and 3, respectively; sCD16, soluble fragment of human FcγRIII; TBS, Tris-buffered saline [20 mM Tris (pH 7.5) and 140 mM NaCl]; PBS, phosphate-buffered saline [140 mM NaCl, 1.5 mM KH_2PO_4, and 8.1 mM Na_2HPO_4 (pH 7.4)]; PCR, polymerase chain reaction; RT-PCR, reverse transcriptase PCR; GH, growth hormone; GHbp, growth hormone receptor.

S0006-2960(96)01231-7 CCC: $14.00

As with other lectins that are associated into trimers by the formation of α-helical coiled-coil or collagen stalks (Hoppe & Reid, 1994), the avidity of CD23 may be achieved by the cooperative binding of more than one lectin domain to IgE. There are two identical ϵ-heavy chains in IgE and the structure has been predicted to have 2-fold rotational symmetry (Padlan & Davies, 1986; Helm et al., 1991), at least within the Cϵ3 and Cϵ4 domains. The CD23 binding site in IgE has been mapped to Cϵ3, and we have suggested that two lectin domains may bind at identical sites on the two Cϵ3 domains (Sutton & Gould, 1993).

Both to simplify the task of studying the interaction with IgE and to study a functionally important biological interaction, we have expressed the 16 kDa lectin fragment (sCD23) in cells of the NS-0 (mouse myeloma) cell line. We have studied the interaction of this monomeric fragment with the smallest fragment of IgE, a dimer of the Cϵ3 and Cϵ4 domains (Fcϵ3−4), which we find interacts with native CD23 with essentially the same affinity as IgE (Young et al., 1995). We have used sedimentation equilibrium in the analytical centrifuge to measure the association constant(s), stoichiometry, and thermodynamics of the binding of the monomeric unit(s) to IgE.

This study has uncovered an unexpected feature of the binding of sCD23 to IgE. The stoichiometery of binding is indeed, as predicted, 2:1 (sCD23:Fcϵ3−4). The two binding events (binding of the first and second molecule of sCD23), however, have strikingly different thermodynamics, leading to the conclusion that the two binding sites are different and that the second molecule of sCD23 recognizes a site on IgE that is not available before the first molecule of sCD23 binds. Molecular modeling supports the conclusion that there must be two different CD23 binding sites in IgE and leads to the further conclusion that the corresponding sites in the dimeric/trimeric CD23 must also differ from one another.

MATERIALS AND METHODS

Preparation and Isolation of 16 kDa sCD23. The CD23 cDNA sequence in pUC18 from J. Yodoi (Kyoto University, Kyoto, Japan) (Ikuta et al., 1987) was used as a template for the PCR to generate the DNA fragment corresponding to the 16 kDa recombinant lectin domain fragment of human CD23. Two oligonucleotides for PCR were synthesized on the basis of the cDNA sequence, to engineer half an *Eco*RV restriction site at the 5′ end of the forward primer (5′ATC-GAGTTGCAGGTGTCCAGCGGC), and a stop codon and a *Bam*HI site at the 5′ end of the reverse primer (5′TCG-GATCCTCAGCATGTGGCCAGCCG). For the PCR mixtures, containing each primer at 1 μM, 0.25 mM dNTPs, and T11 DNA polymerase (1 unit per 50 μL of reaction mixture) in the buffer supplied (Promega), 30 cycles were performed, using a denaturation cycle of 94 °C for 1 min, annealing at 55 °C for 1 min, and extension at 72 °C for 2 min. The PCR product of the expected size was purified by electroelution following gel electrophoresis in 1% agarose. The 5′-phosphorylated and *Bam*HI-restricted DNA fragment was then ligated into the plasmid pRY27 (Young et al., 1995) at the *Eco*RV and *Bam*HI sites, downstream of the antibody B72.3 mouse hybridoma κ-chain leader sequence on the plasmid. This plasmid (pJS10) was transformed into competent TG1 *Escherichia coli* using the $CaCl_2$ method, and plasmids isolated from single colonies were subjected to double-stranded DNA sequencing. The fragment of CD23 with the κ-chain leader sequence was released from pJS10 by a *Eco*RI and *Bam*HI digestion and subcloned into the pJA97 (Celltech) expression vector and subsequently into the pEE12 (Cockett et al., 1990; Bebbington et al., 1992) expression vector at the *Eco*RI and *Bam*HI sites. The vector was then permanently transfected into NS-0 cells as follows. Ten million exponentially growing NS-0 cells were pelleted, washed twice with ice-cold PBS, and resuspended in 0.7 mL of ice-cold PBS. The linearized expression plasmid (40 μg) was mixed with the cell suspension, kept on ice for 5 min, and electroporated in a 0.4 mL electroporation cuvette (Bio-Rad) with two consecutive 0.1 s pulses of 1500 V at 3.0 μF. The cells were returned to ice for 5 min and then resuspended in 140 mL of CB2 DMEM (Gibco, Paisley, U.K.) supplemented with 10% (v:v) fetal calf serum, penicillin (10 units/mL), and streptomycin (10 μg/mL). The cells were plated out into 96-well tissue culture plates at 100 μL per well, left overnight at 37 °C, treated with 100 μL of 10 μM methionine sulfoxamine (Sigma) in CB2 DMEM (Gibco, U.K.) supplemented with 10% (v:v) fetal calf serum, penicillin (10 units/mL), and streptomycin (10 μg/mL), and left for a further 2−3 weeks at 37 °C. Protein expression was analyzed by Western blotting, utilizing the biotinylated anti-CD23 monoclonal antibody BU38 (Binding Site, Birmingham, U.K.) and ELISA assay. The NS-0 cells secreting 16 kDa sCD23 were cultured in 2 L rolling flasks (Corning, Corning, NY) using CB2 DMEM supplemented with 10% (v:v) fetal calf serum, penicillin (10 units/mL), streptomycin (10 μg/mL), and 1 mM L-glutamine, to confluence. The supernatants were harvested and filtered through 0.45 μm filters (Amicon, Beverley, MA) immediately following centrifugation. The recombinant sCD23 was purified on an anti-CD23 monoclonal antibody (MHM6) affinity column (Sepharose, Pharmacia), eluted with 0.1 M glycine (pH 2.5), and immediately neutralized with an appropriate volume of 1 M Tris. The protein was then HPLC purified on a Superdex 75 HR 20/30 column (Pharmacia, Sweden) using TBS containing 2 mM $CaCl_2$.

Preparation of the IgG−sFcϵRIα Fusion Protein. A soluble fragment of the high-affinity IgE receptor α-chain fused to the Fc region of IgG_4 (sFcϵRIα−IgG_4Fc) was used for affinity purification and was prepared as follows. The gene segment encoding the extracellular domains of FcϵRIα was isolated on a *Hin*dIII-*Sal*I fragment from full length α-chain cDNA by PCR. The plasmid MRR14 containing a human γ4 genomic clone was modified by site-directed mutagenesis to incorporate a *Sal*I site toward the 3′ end of the CH1 domain. A *Sal*I-*Eco*RI fragment containing the 3′ end of the CH1, hinge, CH2, and CH3 exons was isolated from this plasmid, and the α and γ4 sequences, fused through the *Sal*I sites (sequence PREK/VDKRV at the α2/Cγ1 junction), were inserted into the *Hin*dIII-*Eco*RI sites of the expression vector PEE12 (Cockett et al., 1990; Bebbington et al., 1992). PEE12 was transfected into NS-0 cells and permanent cell lines screened by ELISA using plates coated in anti-IgG4 (MC007, The Binding Site, Birmingham, UK) and an anti-IgG HRP conjugate (800−367−5296, Jackson). IgG_4−Fc−(sFcϵRIα)$_2$ was affinity purified on a protein A-Sepharose column (Pharmacia).

Preparation of Fcϵ3−4. The cDNA sequence encoding the ϵ-chain of human IgE (Kenten et al., 1982) from C328 to K547 was amplified from 25 ng of the pRY22 template

[which contains the mutations C255A, N265Q, and N371Q (Young et al., 1995)]. C328 and A329 are the last two amino acids in Cε2, so the product encodes all of the Cε3 and Cε4 domains in addition to these two residues at the amino terminus. The PCR was performed in a 100 μL reaction volume using 20 cycles of 94 °C for 1 min, 62 °C for 1 min, and 72 °C for 1 min. The primer 5′ATCTGTGCAGATTCCAACCCGAGA was used to amplify the 5′ end of the Cε3 sequence, and the plasmid-specific primer 5′CAAATGTGGTATGGCTGA was used to amplify the 3′ end of the construct. A product containing an *Eco*RV end with an extra dipeptide DI immediately preceding C328 was amplified. This modification allowed the PCR product to be ligated to a light chain leader sequence, and subsequent leader processing when the construct was expressed (Young et al., 1995). The PCR fragment was cut downstream of the IgE polyadenylation sequence with *Hin*dIII and then ligated along with an *Eco*RI-*Eco*RV restriction fragment containing the light chain leader sequence (Young et al., 1995) into *Eco*RI-*Hin*dIII-restricted pSP64 (Promega). An *Eco*RI-*Nhe*I restriction fragment containing the construct was cut from this vector and ligated into an NS-0 cell expression vector, and stable NS-0 lines were established as described [see above and Young et al. (1995)]. The human IgE Fcε3−4 protein was purified from tissue culture supernatant on a sFcεRIα−IgG Fc fusion protein affinity column (Sepharose, Pharmacia, Sweden), eluted with 0.1 M glycine (pH 2.5), and immediately neutralized with 1 M Tris. The protein was then HPLC purified on a Superdex 75 HR 10/30 column (Pharmacia, Sweden) using 50 mM sodium phosphate, 150 mM sodium chloride, 500 mM arginine chloride (pH 6.0), and 0.05% NaN_3. Samples were dialyzed into other buffers as required.

Characterization of sCD23 and Fcε3−4. The purity and molecular mass of the sCD23 and Fcε3−4 preparations were verified by SDS−PAGE under reducing and nonreducing conditions (Laemmli, 1970) and analytical ultracentrifugation. The concentrations of the Fcε3−4 and sCD23 solutions were determined using calculated extinction coefficients at 280 nm of 64 520 and 45 180 M^{-1} cm^{-1}, respectively, based on the amino acid composition (Wetlaufer, 1962). Circular dichroism spectra were measured in millidegrees for both sCD23 and Fcε3−4 using a Jobin-Yvon CD-6 spectropolarimeter as follows. The samples were dialyzed into 10 mM potassium phosphate at pH 7.5, placed in cylindrical quartz cells (Hellma) with a path length of 0.5 mm, and scanned from 195 to 260 nm at 10 °C. The data were corrected by subtraction of the solvent spectrum obtained under identical conditions and converted to Δε in liters per molar per centimeter per backbone amide. Graphs were plotted using Origin 4.0 (Microcal Software Inc., Northampton, MA), and the percentages of α-helix, β-sheet, and random coil structure were calculated using the program CONTIN (Provencher & Glockner, 1981). Cell binding assays were used to assess the affinity of binding of Fcε3−4 to both native membrane-bound CD23 on the RPMI 8866 B cell line and recombinant high-affinity receptor FcεRIα expressed in CHO cells, using methods described previously (Young et al., 1995.)

Sedimentation Equilibrium Studies. Analytical ultracentrifugation experiments were performed using a Beckman XL-A analytical ultracentrifuge, as previously described (Ghirlando et al., 1995). Sedimentation equilibrium experiments on Fcε3−4 were conducted at various rotor speeds, ranging from 16 000 to 20 000 rpm, and 4.0 °C, whereas experiments on sCD23 were conducted at rotor speeds ranging from 18 000 to 26 000 rpm. Experiments to determine the temperature dependence of the buoyant molecular masses of Fcε3−4 and sCD23 were performed in TBS and 2 mM $CaCl_2$ at 18 000 rpm and temperatures ranging from 1.0 to 19.0 °C. Data were analyzed in terms of a single ideal solute to obtain the buoyant molecular mass, $M(1 - \bar{\nu}\rho)$, as described (Ghirlando et al., 1995). Residuals were calculated by subtracting the best fit of the model from the experimental data. In all cases, a random distribution of the residuals around zero was noted as a function of the radius.

Experiments to study the interactions between sCD23 and Fcε3−4 were carried out as described for IgG_1−Fc and sCD16 (Ghirlando et al., 1995). Data were collected at a rotor speed of 18 000 rpm and temperatures in the range of 1.0 to 19.0 °C in TBS and 2 mM $CaCl_2$. Data analyses by mathematical modeling were performed using Sigma Plot 4.16 (Jandel Scientific, San Rafael, CA) operating on a Power Macintosh 7100/66 computer. Simultaneous weighted nonlinear least-squares fitting of the data sets at each temperature was performed using different mathematical models of the following form:

$$A_r = A_{o,A}\exp[HM_A(r^2 - r_o^2)] + A_{o,B}\exp[HM_B(r^2 - r_o^2)] + A_{o,A}A_{o,B}\exp[\ln k_{01} + H(M_A + M_B)(r^2 - r_o^2)] + A_{o,A}(A_{o,B})^2\exp(\ln k_{02} + H(M_A + 2M_B)(r^2 - r_o^2)] + E \quad (1)$$

where $A_{o,A}$ is the absorbance of Fcε3−4 at a reference point r_o and $A_{o,B}$ is the absorbance of sCD23 at the reference point r_o. The values of M_A and M_B represent the experimentally determined buoyant molecular masses for Fcε3−4 and sCD23, respectively. It is assumed that no changes in the partial specific volume occur upon complex formation and that the buoyant molecular mass of a complex is the sum of that of the components. The apparent equilibrium constants k_{01}, for the 1:1 association, and k_{02}, for the 1:2 association of free Fcε3−4 and sCD23 (Figure 1), are on an absorbance concentration scale. A_r, H, and E have been previously defined (Ghirlando et al., 1995). These models have the equilibrium constant(s) as global fitting parameter(s) and cell reference concentrations and baseline corrections as local fitting parameters. Data fitting was done on two sets of data to yield average values of ln k_{01} and ln k_{02}.

Thermodynamic Analysis. The values of ln k_{01} and ln k_{02} obtained by data modeling were converted to ln K_{01} and ln K_{02} values, K_{01} and K_{02} now being association constants on a molar scale, using the extinction coefficients calculated for the Fcε3−4 dimer and sCD23. The corresponding free energies ΔG°_{01} and ΔG°_{02} at each temperature investigated, describing the overall 1:1 and 2:1 associations, respectively, were then calculated:

$$\Delta G^\circ = -RT\ln K \quad (2)$$

It is assumed that the dimeric Fcε3−4 chain possesses two identical and symmetrically related binding sites for the first sCD23 species. As shown in Figure 1 [using the nomenclature of Weber (1975), as described in Cantor and Schimmel (1980)], this leads to identical values of K_1 and K_2, these being the association constants for the formation of Fcε3−4−sCD23 and sCD23−Fcε3−4 respectively. Ac-

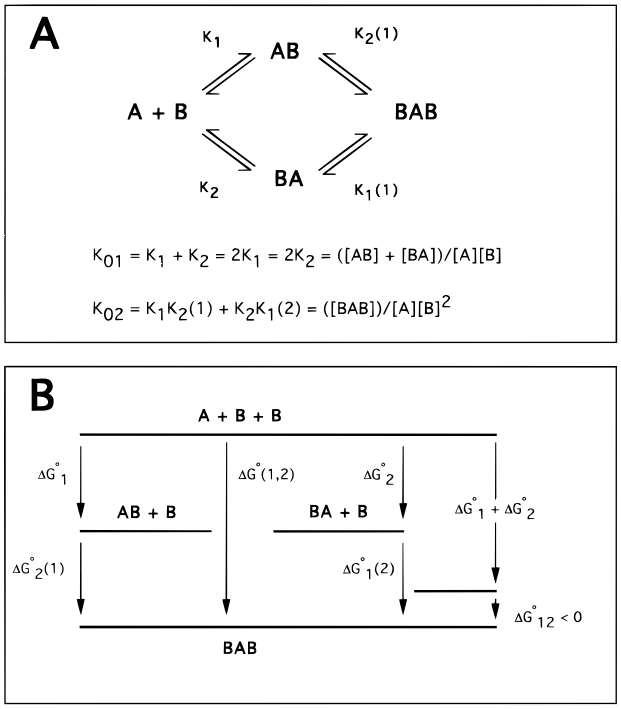

FIGURE 1: Reaction and free energy diagram for a system of two sCD23 molecules (B) with one Fcε3−4 fragment (A). (A) Reaction scheme for the 1:1 and 2:1 association of sCD23 with Fcε3−4. The association constants K_1, K_2, $K_2(1)$, and $K_1(2)$ are defined. Analytical ultracentrifugation only allows for a distinction of associating species based on their molecular mass, leading to the apparent association constants K_{01} and K_{02} for 1:1 and 2:1 complex formation, respectively. On the basis of symmetry considerations, the complexes AB and BA are equivalent, leading to the relations between K_{01}, K_1, and K_2, as well as between K_{02}, $K_1K_2(1)$, and K_2K_1-(2) shown. (B) Free energy diagram for the 1:1 and 2:1 association of sCD23 with Fcε3−4. The labeled states define the sum of the standard chemical potentials of the particular species. The notation for the free energy changes follows that used for the association constants. The coupling free energy, $\Delta G°_{12}$, is defined as shown. It represents the difference between the standard free energy for the overall reaction to BAB and the sum of the standard free energies for the reactions A + B = AB and A + B = BA [after Weber (1975) and Cantor and Schimmel (1980)]. The notation for $\Delta H°$, ΔS, and $\Delta Cp°$ follows that for $\Delta G°$.

cordingly, on the basis of the relations between K_1, K_2, and the overall constant K_{01}, it follows that

$$\Delta G°_1 = \Delta G°_2 = \Delta G°_{01} + RT \ln 2 \qquad (3)$$

$\Delta G°_{02}$ returned from the sedimentation equilibrium data is equivalent to $\Delta G°(1,2)$ (Figure 1), which is the overall free energy for binding the first and second sCD23 molecules to Fcε3−4. The coupling free energy, $\Delta G°_{12}$, which indicates the mutual effect of the one sCD23 on the other, is defined in Figure 1. It is the difference between the standard free energy for the overall reaction to sCD23−Fcε3−4−sCD23 and the sum of the standard free energies $\Delta G°_1$ and $\Delta G°_2$. The values of $\Delta G°_1(2)$ and $\Delta G°_2(1)$ are identical on the basis of symmetry considerations. These describe the association of a second sCD23 species with Fcε3−4−sCD23 and sCD23−Fcε3−4, respectively, and were calculated from the difference of $\Delta G°(1,2)$ and $\Delta G°_1 = \Delta G°_2$.

The enthalpies ($\Delta H°$), entropies ($\Delta S°$) and changes in the heat capacity of association ($\Delta C_p°$) for the 1:1 association of Fcε3−4 with sCD23 and the association of the 1:1 Fcε3−4−sCD23 complex with a further sCD23 molecule were obtained by fitting the data for $\Delta G°_1$ and $\Delta G°_1(2)$ to

$$\Delta G° = \Delta H°_{T_o} - T\Delta S°_{T_o} + (T - T_o)\Delta C_p° - T\Delta C_p° \ln(T/T_o) \quad (4)$$

using a reference temperature T_o of 273.15 K. It is assumed that $\Delta C_p°$ is a temperature-independent variable (Yoo & Lewis, 1995).

Sedimentation Velocity Studies. Sedimentation velocity experiments were performed at 20.0 °C on the Beckman Optima XL-A instrument at different rotor speeds ranging from 40 000 to 50 000 rpm in the case of Fcε3−4 or 50 000 to 60 000 rpm for sCD23. Loading concentrations corresponding to initial measured A_{280} values of 0.8 (Fcε3−4 in PBS and 0.05% NaN_3) and 0.7 (sCD23 in TBS and 2 mM $CaCl_2$) were used. Data were acquired as single absorbance measurements at a nominal wavelength of 280 nm and a radial spacing of 0.003 cm and analyzed with the program XLAVEL (Beckman) to yield the uncorrected sedimentation coefficient. Data from several runs were averaged and corrected to obtain $s_{20,w}$ as previously described (Keown et al., 1995).

Hydrodynamic Modeling. The sedimentation coefficient for Fcε3−4 was computed on the basis of models of the structure of IgE−Fc (Padlan & Davies, 1986; Helm et al., 1991), using carbohydrate chains modeled on those found in the human IgG−Fc crystal structure (Deisenhofer, 1981) as described previously (Keown et al., 1995; Beavil, A. J., et al., 1995). Similarly, the sedimentation coefficient for the sCD23 was computed by modeling this putative C-type lectin domain on the basis of the structure of the homologous domain reported for the mannose binding protein (Weis et al., 1991, 1992; Padlan & Helm, 1993).

RESULTS

Fcε3−4 and sCD23 Are Pure and Monodisperse. The purity of the protein preparations was assessed by reducing and nonreducing SDS−PAGE (Laemmli, 1970) (Figure 2a). sCD23 migrates as a single band with an apparent molecular mass of 16 kDa under both reducing and nonreducing conditions. Under nonreducing conditions, the Fcε3−4 preparation showed two bands corresponding to a dimer (apparent molecular mass of 55 000 Da) and a monomer (apparent molecular mass of 30 000 Da), indicating that approximately 90% of the Fcε3−4 preparation contains the native interchain disulfide link C328 connecting the N termini of the two Cε3 domains. Under reducing conditions, a single monomeric band is observed. Sedimentation equilibrium was used to determine the molecular mass of the protein fragments (Figure 2b, Table 1). These experiments give the buoyant molecular mass $M(1 - \bar{\nu}\rho)$ and give information on the polydispersity of the samples. The sedimentation equilibrium distribution for sCD23 (Figure 2b, part A) shows that this preparation is monodisperse, within the experimental precision of the method. Using the calculated partial specific volume ($\bar{\nu}$) of 0.719 $cm^3\ g^{-1}$, based on the amino acid composition (Perkins, 1986), the experimentally determined $M(1 - \bar{\nu}\rho)$ of 4750 ± 140 g mol^{-1} at 19 °C corresponds to a molecular mass of 16 900 ± 500 g mol^{-1}. This is larger than the molecular mass of 15 757 g mol^{-1} calculated from the amino acid composition alone. Since the same buoyant molecular mass is obtained at various rotor speeds, the larger

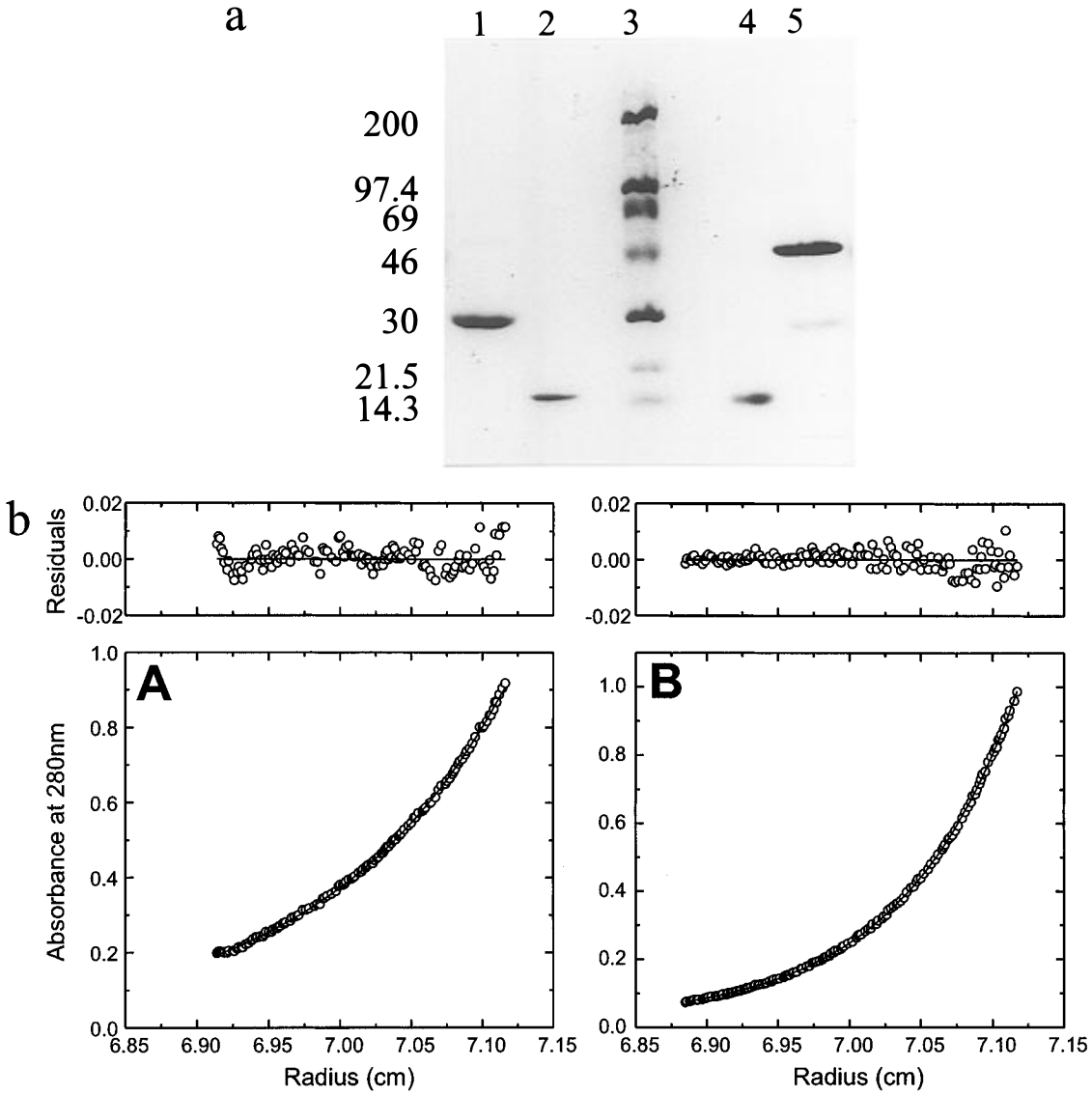

FIGURE 2: Recombinant sCD23 and Fcϵ3−4 are single, monodisperse species. (a) Five to twenty percent gradient SDS−PAGE of Fcϵ3−4 and sCD23, reducing and nonreducing: lane 1, Fcϵ3−4 reduced; lane 2, sCD23 reduced; lane 3, molecular mass markers; lane 4, sCD23 nonreduced; and lane 5, Fcϵ3−4 nonreduced. (b) Sedimentation equilibrium data for sCD23 and Fcϵ3−4, shown as a distribution of A_{280} at equilibrium. Data were collected at 4.0 °C and 22 000 rpm for sCD23 (A) and 16 000 rpm for Fcϵ3−4 (B). The results are analyzed for the best single-component $M(1 - \bar{\nu}\rho)$ fit, shown as a line through the experimental points. Corresponding distributions of the residuals are shown above each plot.

Table 1: Sedimentation Equilibrium and Velocity Data

sample	$M(1 - \bar{\nu}\rho)$ (g mol^{-1})[a]	M_{exp} (g mol^{-1})[b]	$(d\bar{\nu}/dt)/10^{-4}$ (cm^3 g^{-1} K^{-1})	experimental $s_{20,w}$[a]	modeled $s°_{20,w}$[c]
sCD23	4870 ± 160 (3)	15757	7.3 ± 0.7	1.92 ± 0.05 (3)	1.95
Fcϵ3−4	14000 ± 300 (9)	52200 ± 900	4.2 ± 1.0	3.77 ± 0.05 (5)	3.85

[a] Experimentally determined mean values based on *n* measurements (*n* shown in parentheses) together with the standard error. Buoyant molecular masses were measured at 4.0 °C, and experimental $s_{20,w}$ data are based on data collected at 20.0 °C. [b] Measured values of the molecular mass based on the experimental values of $M(1 - \bar{\nu}\rho)$, calculated as described in eq 5 (Ghirlando et al., 1995). In the case of sCD23, the value of the partial specific volume was obtained on the basis of the protein molecular mass directly. [c] Modeled values obtained as described in the text.

molecular mass calculated is not due to self-association of sCD23. In addition, no evidence for glycosylation was found experimentally (data not shown); therefore, the large value of $M(1 - \bar{\nu}\rho)$ is a reflection of a smaller than calculated $\bar{\nu}$. On the basis of the buoyant molecular mass at 19 °C, an experimental value for $\bar{\nu}$ is calculated to be 0.695 ± 0.009 cm^3 g^{-1}.

Sedimentation equilibrium data for the Fcϵ3−4 (Figure 2b, part B) indicated that this preparation is also monodisperse within the experimental precision of the technique. The molecular mass was calculated from $M(1 - \bar{\nu}\rho)$ using the $\bar{\nu}$ for the protein component (p) calculated from the amino acid composition (Perkins, 1986) and the $\bar{\nu}$ of 0.65 cm^3 g^{-1} for the carbohydrate component (c) (Durchschlag, 1986) according to eq 5 (Ghirlando et al., 1995).

$$M(1 - \bar{\nu}\rho) = M(1 - \bar{\nu}_c\rho) + M_p(\bar{\nu}_c - \bar{\nu}_p)\rho \qquad (5)$$

The calculated molecular mass is 52 200 ± 900 g mol^{-1}, within experimental error of the value of 52 797 g mol^{-1} predicted for dimeric Fcϵ3−4 with full occupancy of the glycosylation sites. It therefore appears that, although 10%

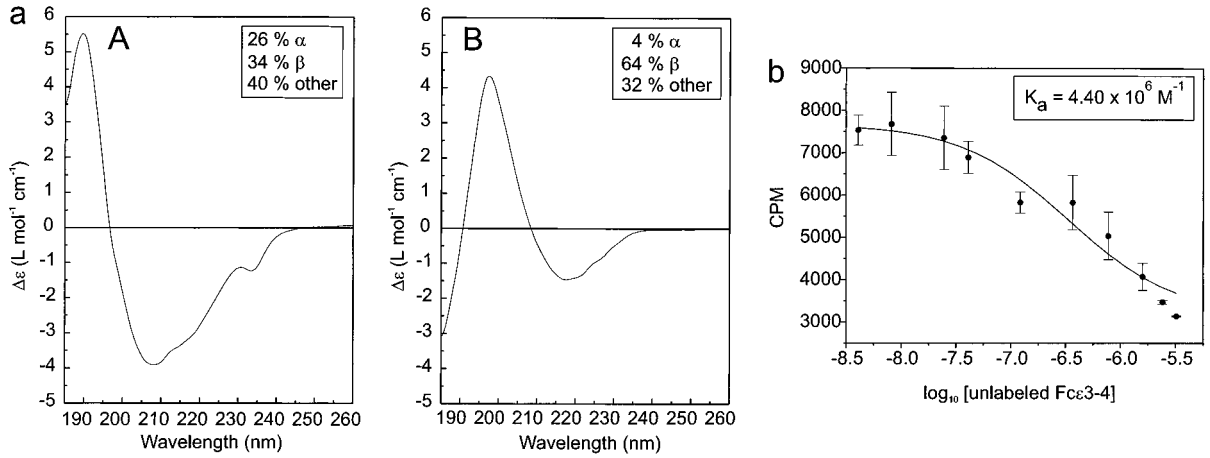

FIGURE 3: sCD23 and Fcε3−4 are fully folded and active. (a) Circular dichroism spectra of sCD23 (A) and Fcε3−4 (B). The curves were analyzed using CONTIN (Provencher & Glockner, 1981), and the predicted values of α-helix, β-sheet, and other structure are indicated. (b) A representative set of binding assay data and the corresponding association constant for Fcε3−4 binding to membrane CD23 on RPMI 8866 cells as previously described for IgE−Fc (Young et al., 1995). The experiment was performed in duplicate, and the values were averaged, with the error bars indicating the range between data points.

of the preparation does not contain the disulfide link (Figure 1a), it is still dimeric.

Fcε3−4 and sCD23 Are Fully Folded and Active. Circular dichroism spectra were measured for Fcε3−4 and sCD23 (Figure 3a), and the amount of secondary structure was calculated using CONTIN (Provencher & Glockner, 1981). The values indicate that Fcε3−4 is composed mostly of β-sheet, as predicted for a correctly folded immunoglobulin domain. This indicates that loss of the Cε2 domains does not destabilize either of the Cε3 or Cε4 domains. The values measured for sCD23 are consistent with secondary structural elements similar to those in the related mannose binding protein (Weis et al., 1991). Cell binding studies indicate that Fcε3−4 binds to membrane CD23, with a K_a of $(5.9 \pm 2.3) \times 10^6$ M^{-1}, and a representative set of binding data is shown in Figure 3b. In addition, Fcε3−4 binds to the high-affinity receptor FcεRI with a K_a of 9×10^{10} M^{-1} (Keown et al., 1997), and both of these values are comparable to those previously published for recombinant IgE−Fc (Young et al., 1995).

The experimentally determined values of $\bar{\nu}$ for Fcε3−4 and sCD23, derived from measurements of the buoyant molecular masses, vary linearly with temperature in the range from 1 to 19 °C (Figure 4). Fcε3−4 yields a slope ($d\bar{\nu}/dT$) of 4.2×10^{-4} cm^3 g^{-1} K^{-1}, and sCD23 is characterized by a $d\bar{\nu}/dT$ of 7.3×10^{-4} cm^3 g^{-1} K^{-1} (Table 1). A linear dependence of $\bar{\nu}$ with temperature has been observed for a number of proteins [reviewed in Durchschlag (1986)] with an average $d\bar{\nu}/dT$ of 4.25×10^{-4} cm^3 g^{-1} K^{-1}, a value identical to that measured for Fcε3−4. Interestingly, Fcε3−4 gives a value which is slightly smaller than that reported for IgG_1−Fc (Ghirlando et al., 1995), a similar two domain disulfide linker dimer. sCD23 gives a value of $d\bar{\nu}/dT$ which is larger than typically found but is within the range reported for various proteins (Durchschlag, 1986). Large values of $d\bar{\nu}/dT$ can be indicative of unfolded protein states (Durschschlag, 1986), but the data for Fcε3−4 and sCD23 suggest that both these protein preparations are fully folded.

The compact nature of these proteins has also been verified using sedimentation velocity studies. Sedimentation coefficients ($s_{20,w}$) were measured experimentally (Table 1) and compared to those calculated on the basis of models of

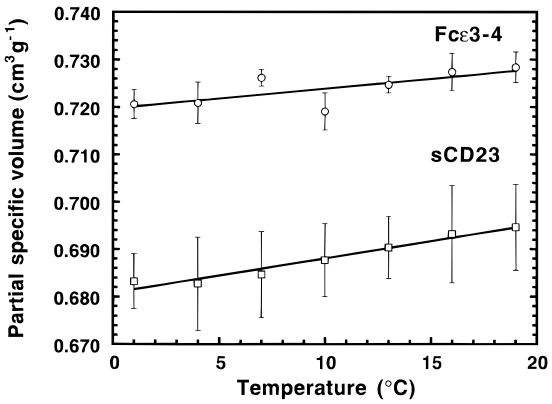

FIGURE 4: Variation of partial specific volume with temperature. Experimentally determined values of the partial specific volume $\bar{\nu}$ for sCD23 and Fcε3−4 in TBS and 2 mM $CaCl_2$ as a function of the temperature, calculated from the concentration distribution at equilibrium at a rotor speed of 16 000 rpm. The loading concentrations were an A_{280} of 0.5. The error is based on the standard error of the buoyant molecular mass returned from the fit to eq 1. The best fit straight lines to the data are as follows: $\bar{\nu} = 0.730 + [4.2 \times 10^{-4}T$ (in degrees Celsius)] ($R^2 = 0.85$) for Fcε3−4 and $\bar{\nu} = 0.681 + [7.3 \times 10^{-4}T$ (in degrees Celsius)] ($R^2 = 0.98$) for sCD23.

homologous systems. Calculated $s°_{20,w}$ values for Fcε3−4 were based on IgE−Fc models (Padlan & Davies, 1986; Helm et al., 1991) and for sCD23 were based on data from the crystal structure of mannose binding protein (Weis et al., 1991, 1992; Padlan & Helm, 1993). The calculated $s°_{20,w}$ values are identical, within experimental error, to the measured values (Table 1) and confirm that both proteins are compact structures. All of these data suggest that both protein fragments adopt a native conformation in solution.

sCD23 and Fcε3−4 Interact To Form 1:1 and 2:1 Complexes. In order to establish the stoichiometry of possible sCD23 and Fcε3−4 complexes, a series of sedimentation equilibrium experiments were carried out on mixtures of the two components. Three different sCD23: Fcε3−4 loading ratios, corresponding to 1:2, 1:1, and 2:1, were studied simultaneously at various temperatures. The sedimentation equilibrium data from the three different loading ratios were fitted simultaneously to various models, on the basis of the formation of 1:1 or 2:1 complexes of sCD23−Fcε3−4. The data were initially fitted to models

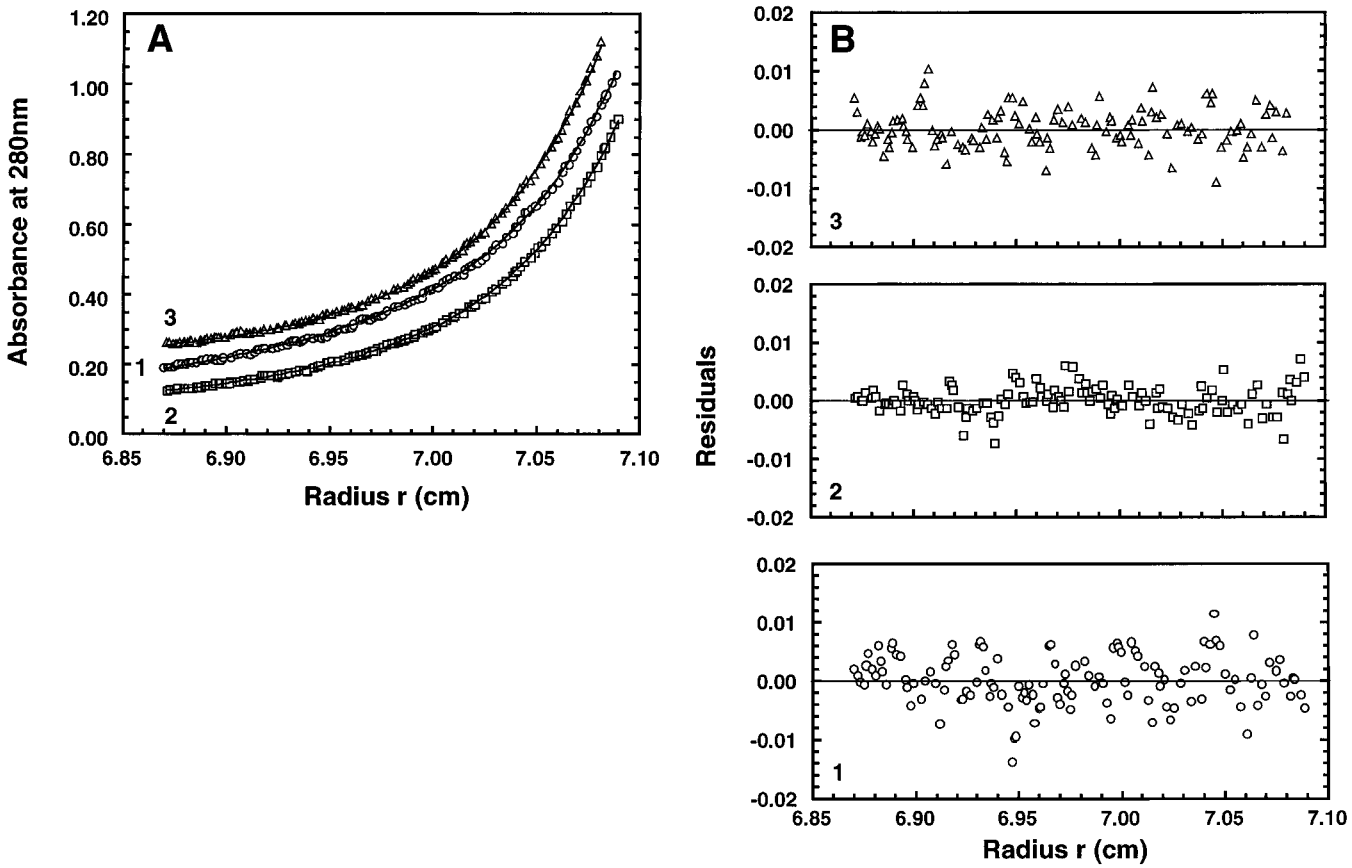

FIGURE 5: Formation of 1:1 and 2:1 complexes of sCD23 and Fcϵ3−4. Sedimentation equilibrium profiles at 280 nm, and the corresponding residuals, for mixtures of sCD23 and Fcϵ3−4 at 16 000 rpm and 16.0 °C. The symbols correspond to the following sCD23:Fcϵ3−4 ratios: 1 (circles), 2:1; 2 (squares), 1:1; and 3 (triangles), 1:2. The initial concentrations corresponded to a combined A_{280} of 0.5. (A) Sedimentation equilibrium profiles at 280 nm. The data for 3 have been shifted by $+0.15A_{280}$ for clarity. The lines through the data are the best fit for a reversible 2:1 association. (B) Distribution of the residuals for the 2:1 interaction between sCD23 and Fcϵ3−4.

in which sCD23 and Fcϵ3−4 interact to form only 1:1 complexes (corresponding to eq 1 with the last term containing ln k_{02} removed) or 2:1 complexes (corresponding to eq 1 with the term containing ln k_{01} removed). In both cases, a nonrandom residual distribution was observed (Figure 6) and a corresponding minimum sum of squares of 6.2×10^{-3} was obtained for each at 16.0 °C. When the data were fitted to the model described by eq 1, that is, allowing for the formation of both 1:1 and 2:1 complexes, an excellent fit to the experimental data was obtained with an improved residual distribution (Figure 5) and a minimum sum of squares value of 4.2×10^{-3}. Indeed, this model yields an excellent fit to the data at all temperatures, returning ln K_{01} and ln K_{02} values of 12.7 ± 0.21 and 24.3 ± 0.15 at 1.0 °C, respectively, and 12.2 ± 0.19 and 23.4 ± 0.07 at 19.0 °C, respectively. Figure 5A shows the best fit to the data at 16.0 °C using this model. The corresponding residuals (Figure 5B) are typical of those obtained at various temperatures and illustrate the validity of this model. We note, furthermore, that the residuals of the best fit (Figure 5B) were found to be normally distributed at all temperatures studied (data not shown). To further test the validity of this model, the data were also fitted using a model in which sCD23 and Fcϵ3−4 associate to form 1:1, 2:1, and even 3:1 complexes [corresponding to eq 1 with an additional term of the form $A_{o,A}(A_{o,B})^3 \exp[\ln k_{03} + H(M_A + 3M_B)(r^2 - r_o^2)]$, where k_{03} is the apparent association constant for 3:1 complex formation]. In this case, the fit returns ln k_{01} and ln k_{02} values identical to those obtained for the 1:1 and 2:1 association. A ln k_{03} value of less than −60 (corresponding to a ln K_{03} value of −29) is returned, showing that sCD23 and Fcϵ3−4 interact to form only 1:1 and 2:1 complexes. The data were also fitted using a model in which sCD23 and Fcϵ3−4 associate to form a single complex having 3:1 stoichiometry. In this case, nonrandomly distributed residuals (data not shown) were obtained with a sum of squares of 13×10^{-3}. These data illustrate that Fcϵ3−4 only binds a maximum of two sCD23 molecules in a stepwise manner.

Modeling the data in terms of the formation of both 1:1 and 2:1 complexes requires more fitting parameters than that for 1:1 or 2:1 complex formation, and we were concerned that the better fit and lower residuals for formation of both 1:1 and 2:1 complexes may just be a consequence of the increased parameters in eq 1. Such an effect would be compounded by the differences of the buoyant molecular masses of the interacting species (Table 1) and the low-affinity interaction. We note, however, that excellent fits to the data were obtained at all temperatures (Figure 5B and results not shown). To ensure that the data can indeed be modeled or fitted in terms of the formation of both 1:1 and 2:1 complexes, similar experiments were undertaken using three different rotor speeds (14 000, 16 000, and 18 000 rpm) at 1.0 °C. At all rotor speeds investigated, the data were best modeled using eq 1 describing both 1:1 and 2:1 complex formation. Identical values of ln k_{01} and ln k_{02} (within the experimental precision of the method) were returned, justifying the use of this model.

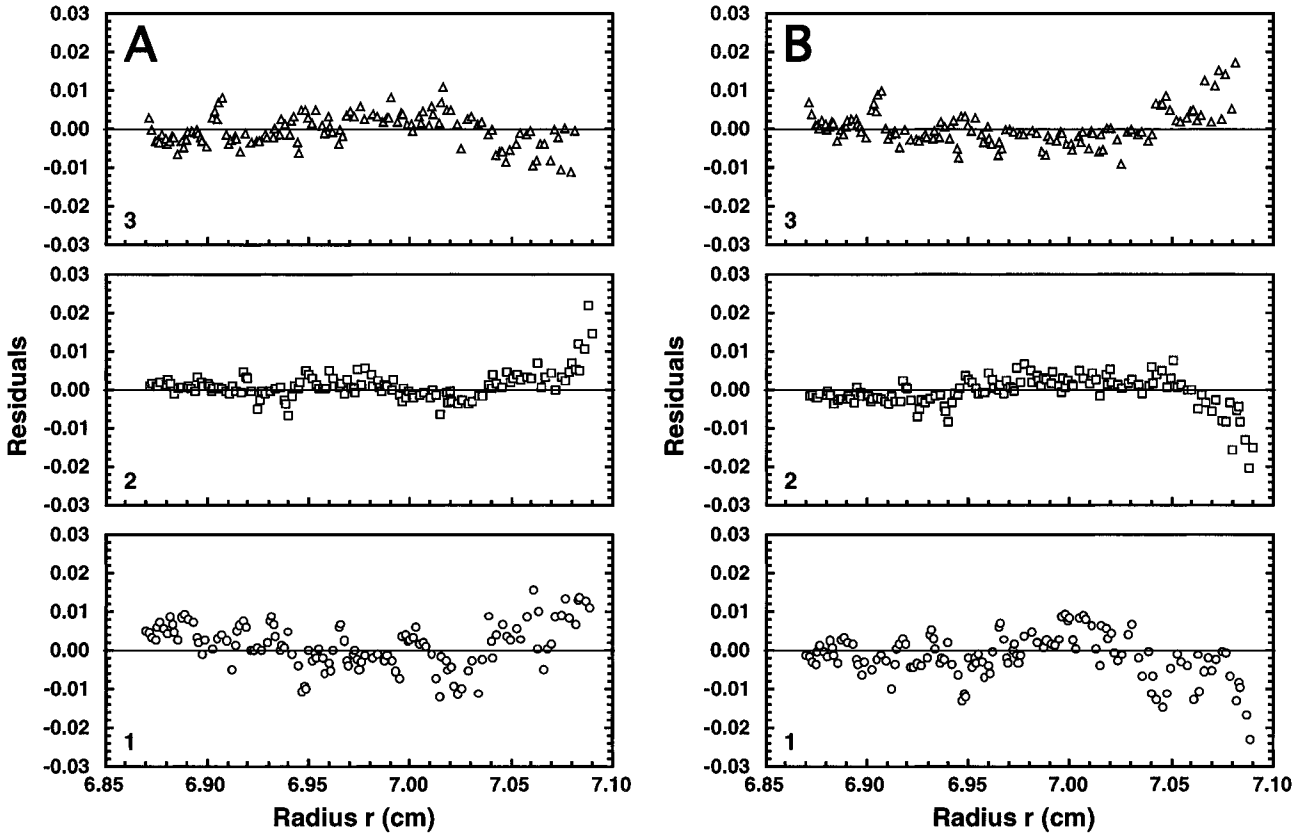

FIGURE 6: sCD23 and Fcε3−4 do not form a single complex. (A) Distribution of the residuals for the 1:1 interaction of sCD23 and Fcε3−4 obtained on the basis of the experimental data in Figure 5A. The symbols correspond to different sCD23 and Fcε3−4 as described in Figure 5. (B) Distribution of the residuals for the 2:1 interaction of sCD23 and Fcε3−4.

Thermodynamics of the Association of sCD23 with Fcε3−4. After the fact that sCD23 and Fcε3−4 associate to form both 1:1 and 2:1 complexes had been established, all of the data were analyzed in terms of this model (eq 1). Using the experimentally observed linear dependence of $\bar{\nu}$ for both sCD23 and Fcε3−4 (Figure 4), and the molecular masses (Table 1), the corresponding values of $M(1 - \bar{\nu}\rho)$ for both components at each temperature were computed. The corresponding values of apparent association constants, for formation of a 1:1 and a 2:1 complex from free reagents (K_{01} and K_{02}, respectively), were then obtained.

Considering that the dimeric Fcε3−4 molecule presents two symmetrically identical binding sites for sCD23, it follows that the value of K_{01} is equal to $2K_1$, or K_2. K_1 and K_2 represent, respectively, the association constants for the formation of symmetric Fcε3−4−sCD23 and sCD23−Fcε3−4 complexes (Figure 1). As both sites are identical, $K_1 = K_2$, which in turn allows for an evaluation of these parameters from K_{01}. The formation of the 2:1 complex from the individual components is described by K_{02}. The values of both K_1 and K_{02} were found to decrease with temperature. K_1 decreases from a nominal value of 1.6×10^5 M^{-1} at 1.0 °C to 0.95×10^5 M^{-1} at 19.0 °C, and K_{02} decreases from a nominal value of 3.4×10^{10} M^{-2} at 1.0 °C to 1.5×10^{10} M^{-2} at 19.0 °C. Temperature-dependent free energy values characterizing the 1:1 association of Fcε3−4 and sCD23 to Fcε3−4−sCD23 or sCD23−Fcε3−4, $\Delta G^\circ_1 = \Delta G^\circ_2$, and the association of the second sCD23, $\Delta G^\circ_1(2) = \Delta G^\circ_2(1)$, were calculated (Figure 1) and fitted to eq 4 to yield the thermodynamic parameters characterizing these associations (Table 2). The corresponding data fits are shown in Figure 7. These parameters are derived on the basis of the assumption of a temperature-independent change of the heat capacity for the association, ΔCp°, leading to temperature-dependent enthalpies and entropies (Yoo & Lewis, 1995). This assumption would appear justified, as fitting the data to an expanded form of eq 4 leads to a zero coefficient for the term in $d(\Delta Cp^\circ)/dT$. In both cases, the thermodynamics are typical of entropy−enthalpy compensation processes in which $|\Delta Cp^\circ| \gg |\Delta S^\circ|$. The associations are both characterized by a favorable enthalpic contribution over most of the temperature range studied, except that the formation of the 1:1 complex has a far larger and favorable $\Delta H^\circ_{T_o}$. The negative value and magnitude of ΔCp°_1 identifies this association process as one in which local folding/rearrangement is coupled to complex formation (Spolar & Record, 1994). The binding of the second sCD23 is mildly cooperative as this is accompanied by a negative coupling free energy value (ΔG°_{12}, Figure 1) at all temperatures studied [i.e. the binding of a second sCD23 species by the 1:1 complex is favored over the formation of a 1:1 complex as depicted in Figure 7, $\Delta G^\circ_2(1) < \Delta G^\circ_1$]. A temperature-averaged coupling free energy ΔG°_{12} of -220 ± 55 cal mol^{-1} is

Table 2: Thermodynamic Parameters for the Association of sCD23 and Fcε3−4

parameters	1:1 association[a]	2:1 association[b]
$\Delta H^\circ_{T_o}$ (kcal mol^{-1})	-2.1 ± 3.3	0.1 ± 5.6
$\Delta S^\circ_{T_0}$ (cal mol^{-1} K^{-1})	16 ± 12	25 ± 20
ΔC_p° (cal mol^{-1} K^{-1})	-320 ± 320	-140 ± 550

[a] Thermodynamic parameters describing the binding of the first sCD23 to Fcε3−4 on the basis of ΔG°_1. [b] Thermodynamic parameters describing the binding of the second sCD23 to the 1:1 complex of sCD23 and Fcε3−4, on the basis of $\Delta G^\circ_2(1)$.

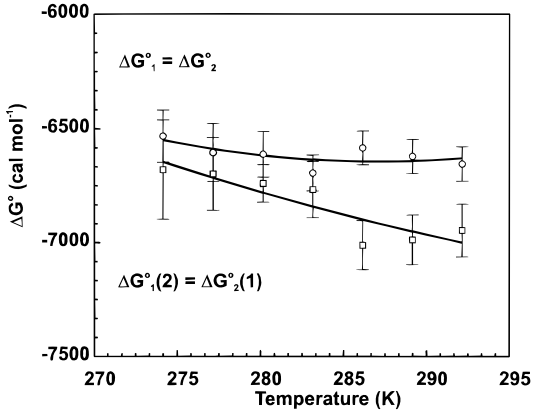

FIGURE 7: Temperature variation of the free energy of association for 1:1 and 2:1 complexes of CD23 with Fcϵ3−4. Temperature dependence of the free energy $\Delta G°$ for the 1:1 association of sCD23 with Fcϵ3−4 ($\Delta G°_1$) and the association of a second sCD23 with the 1:1 sCD23/Fcϵ3−4 complex [$\Delta G°_1(2)$]. The error bars represent the estimated standard error returned from fitting the experimental data. The $\Delta G°_T$ data were fitted to eq 4 with a reference temperature T_o of 273.15 K to yield the parameters in Table 2 and the best fit lines shown.

calculated. This binding event involves a smaller negative change in $\Delta Cp°$ and is characterized by different thermodynamic parameters (Table 2). Unlike the case of $\Delta G°_1$, the data for $\Delta G°_2(1)$ can also be modeled, with an identical correlation coefficient, using a van't Hoff analysis. This leads to temperature-independent $\Delta H°_2(1)$ and $\Delta S°_2(1)$ values of -1.3 ± 1.3 kcal mol^{-1} and 20 ± 5 cal mol^{-1} K^{-1}, respectively. $\Delta Cp°_2(1)$ is necessarily zero. Accordingly, the value computed for $\Delta Cp°_2(1)$ (Table 2) represents a lower limit, and valid values for $\Delta Cp°_2(1)$ are bounded by this and zero. On the basis of the van't Hoff analysis for the $\Delta G°_2(1)$ data, we note that the values of $\Delta H°_2(1)$ and $\Delta S°_2(1)$ are identical (within experimental error) to $\Delta H°_1$ and $\Delta S°_1$ values at 273.15 K. Despite these apparent similarities at low temperatures, the thermodynamics of the 1:1 association are characterized by a significant negative value of $\Delta C_p°$, leading to the observed curvature in $\Delta G°_1$ (Figure 7). This results in different thermodynamics for the binding of the first and second sCD23, as is evident from the data at temperatures above 285 K. On the basis of these differences, the temperatures at which the enthalpic contributions become zero, T_H, are 267 and 272 K, respectively, for the binding of the first and second sCD23. The corresponding entropic contributions are essentially zero at a T_S of 287 and 326 K, respectively.

DISCUSSION

Characterization of Fcϵ3−4 and sCD23. The recombinant fragment of human IgE−Fc, referred to as Fcϵ3−4, encompasses both the Cϵ3 and Cϵ4 domains from residues C328 to K547. This Fcϵ3−4 preparation resembles the Fcϵ (A329−K547) preparation of Basu and co-workers (Basu et al., 1993), who have shown that their preparation (despite the lack of C328) was primarily dimeric, with evidence for both monomer−dimer and dimer−tetramer self-associations. As such associations, presumably a result of the lack of residue C328, would have made our investigations into the interactions more difficult, C328 was retained. Nonreducing SDS−PAGE analysis indicates that at least 90% of the material is covalently dimeric; whereas reducing SDS−PAGE shows the material to be homogeneous (Figure 2a). Sedimentation equilibrium experiments on Fcϵ3−4 clearly demonstrate that the material is monodisperse and dimeric with all N-glycosylation sites fully occupied (Table 1). As has been observed for the homologous IgG$_1$−Fc (Ghirlando et al., 1995), $\bar{\nu}$ for Fcϵ3−4 increases linearly with temperature, in the range of 1.0−19.0 °C, with a slope ($d\bar{\nu}/dT$) of $(4.3 \pm 1.0) \times 10^{-4}$ cm^3 g^{-1} K^{-1} (Figure 4). This, along with the observation that the experimental $s_{20,w}$ value is identical to that calculated on the basis of an Fcϵ3−4 model (Table 1), indicates that Fcϵ3−4 is also folded into a compact state (Durchschlag, 1986). In addition, cell binding assays demonstrate that Fcϵ3−4 binds to membrane CD23 and FcϵRI with affinities similar to those reported for IgE−Fc (Figure 2b; Young et al., 1995), thus confirming that Fcϵ3−4 adopts a native structure.

Recombinant sCD23 comprises the whole of the putative C-type lectin domain involved in the recognition of IgE (Bettler et al., 1992). In the presence of calcium ions, the sCD23 preparation was found to be monodisperse by analytical ultracentrifugation. The linear dependence of $\bar{\nu}$ with temperature indicates that this material is also compact (Figure 4), and the low value of 7.3×10^{-4} cm^3 g^{-1} K^{-1} for $d\bar{\nu}/dT$ may be a reflection of the significant proportion of unstructured residues. On the basis of a comparison with the crystal structure of the rat mannose binding protein (Weis et al., 1991, 1992), the C-lectin domain of human CD23 is expected to contain 19% of the residues in an α-helical conformation and 30% in a β-sheet structure, with most of the remaining residues constituting a central loop held together by calcium ions (Padlan & Helm, 1993). Circular dichroism experiments yield spectra which are consistent with 26% α-helix and 34% β-sheet (Figure 2a). Modeling of sCD23 based on this crystal structure and calculation of the $s°_{20,w}$ value returns a sedimentation coefficient identical to that obtained experimentally (Table 1), indicating that the sCD23 fragment is folded into the correct structure.

Fcϵ3−4 Contains Two Distinct Binding Sites for sCD23. Sedimentation equilibrium data for mixtures of sCD23 and Fcϵ3−4 demonstrate that these species interact with low affinity to form both 1:1 and 2:1 complexes (Figure 5). These observations are consistent with cell binding assays in which murine IgE binding to FcϵRII$^+$ CHO or LPS/IL-4 B blasts was shown to result in a biphasic Scatchard curve (Melewicz et al., 1982; Dierks et al., 1993; Bacon et al., 1993). The lower-affinity binding component was attributed to the interaction of IgE with monomeric CD23 to form a 1:1 complex on the cell surface ($K_a = 2 \times 10^6$ M^{-1} at 4 °C, a value larger than the nominal K_{01} of 3.2×10^5 M^{-1} obtained at 4.0 °C by sedimentation equilibrium in the present study). However, murine sCD23 was found to have an affinity of 10^5−10^6 M^{-1} (Bartlett et al., 1995), similar to the K_a we have determined for human sCD23. The higher affinity binding for membrane CD23 observed by Scatchard analysis (corresponding to a K_a of 1.5×10^8 M^{-1} at 4 °C) was attributed to the binding of IgE to CD23 oligomers on the cell surface (Beavil et al., 1992; Beavil, R. L., et al., 1995). As the oligomerized CD23 contains two or three lectin domains, the higher binding affinity could be explained by the prediction of two binding sites in IgE that lead to cooperative binding (Crothers & Metzger, 1972). The analytical ultracentifugation data unequivocally prove the

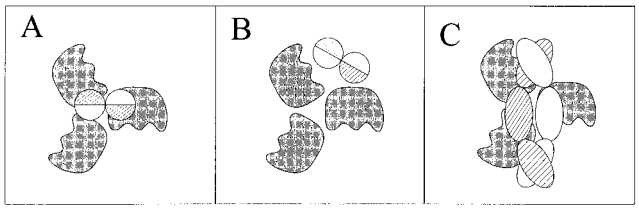

FIGURE 8: Steric constraints on the binding of trimeric CD23 to IgE. The CD23 lectin domain is shown as a shaded, flattened ellipse with wavy and smooth faces, and IgE is shown as two circles to represent the two ϵ-heavy chains. Equivalent faces in each of the IgE chains are shown striped, and CD23 binds to the Cϵ3 domain. Panel A shows the situation where the 2-fold axis of IgE is aligned with the 3-fold axis of CD23. Such an arrangement is impossible, as the Cϵ2 and/or Cϵ3−4 domains cannot be accommodated. Panel B shows a model with the IgE abutting one side of the CD23 trimer, and panel C shows the IgE laying on top of the CD23 with its 2-fold axis perpendicular to the 3-fold axis of CD23. In all cases, it is clearly not possible for the same part on each of the two IgE chains to interact with the same region on CD23, indicating the need to propose two distinct CD23 binding modes. Similar arguments hold for a symmetric CD23 dimer.

existence of two sCD23 binding sites in the Fcϵ3−4 domain of IgE.

The values of $\Delta G°$ characterizing the 1:1 and 2:1 associations [$\Delta G°_1$ and $\Delta G°(1,2)$, respectively (Figure 1)] were used to determine $\Delta G°_2(1)$, the free energy describing the binding of the second sCD23 species, thus allowing for a direct comparison of the first and second binding events (Table 2, Figure 7). The errors in thermodynamic parameters leave open the possibility that the thermodynamics of the interactions of the first sCD23 molecule with Fcϵ3−4 and the second sCD23 with the 1:1 complex are different. The observed values of $\Delta C_p°_1$ and $\Delta C_p°_2(1)$ and the corresponding values of T_S suggest that 1:1 complex formation is accompanied by a larger induced fit/conformational change than 2:1 complex formation (Spolar & Record, 1994), altogether suggesting that Fcϵ3−4 has two distinct binding sites for CD23.

Models of IgE binding to CD23 on the cell membrane (Dierks et al., 1993; Bacon et al., 1993) suggest that two lectin domains can bind to a single IgE molecule. The consequences of a rigid trimeric CD23 with a coiled-coil stalk (Sutton & Gould, 1993), and 3-fold symmetry, binding to a two-chain IgE−Fc are presented in Figure 8. It is sterically impossible for any two of the lectin heads to bind to IgE in the same manner without severe structural distortion, as the regions which contact the IgE in two adjacent heads are on different parts of the lectin domain. These complementary regions on the CD23 lectin head contact one face of the Fc which is composed of opposite sides of the two Cϵ3 domains, resulting in two modes of CD23 lectin binding.

The thermodynamic data presented for formation of a 2:1 complex between sCD23 and Fcϵ3−4 are consistent with this model of oligomeric CD23 binding to IgE (Figure 8). In this model, the CD23 lectin domains interact with one another, as well as with IgE, and it is possible that, in the case of the sCD23−Fcϵ3−4 interaction, the second sCD23 is binding to both Fcϵ3−4 and the first sCD23 molecule. A notable example of such an interaction is the binding of growth hormone receptor (GHbp) to two molecules of growth hormone (GH1 and GH2) (Cunningham et al., 1991). Binding of GH1 generates a new site for the binding of the second growth hormone molecule GH2, which is made up of both GH1 and GHbp. It is tempting to speculate that the binding of one sCD23 molecule (analogous to GH) to IgE (analogous to GHbp) generates a new site for the binding of a second sCD23 that is made up of both IgE and the first molecule of sCD23. Although sCD23 is monomeric, protein−protein cross-linking studies indicate a (weak) tendency for self-association (Beavil, R. L., et al., 1995), and there are certainly contacts between the homologous lectin domains in the crystal structure of mannose binding protein (Weis & Drickamer, 1994; Sherriff et al., 1994). It may be that, on binding to IgE, the two sCD23 lectin domains are interacting with one another in the same way as they would in the trimer, suggesting that as in GH there may also be two binding sites for IgE in the lectin domain of CD23. This would be consistent with the mapping of the IgE binding site on human CD23 to two distinct epitopes on the lectin domain (Bettler et al., 1992). Further studies are required to analyze the structure of the IgE−$(sCD23)_2$ complex.

ACKNOWLEDGMENT

We thank Mr. R. Relić for carbohydrate analysis of sCD23, Dr. G. Mackay for use of unpublished binding data, and Dr. J. Gordon for providing MHM6 antibody. We thank Walter Gratzer and Henryk Eisenberg for helpful discussions.

REFERENCES

Bacon, K., Gauchat, J.-F., Aubry, J.-P., Pochon, S., Graber, P., Henchoz, S., & Bonnefoy, J.-Y. (1993) *Eur. J. Immunol. 23*, 2721−2724.

Bartlett, W. C., Kelly, A. E., Johnson, C. M., & Conrad, D. H. (1995) *J. Immunol. 154*, 4240−4246.

Basu, M., Hakimi, J., Dharm, E., Kondas, J. A., Tsien, W.-H., Pilson, R. S., Lin, P., Gilfillan, A., Haring, P., Braswell, E. H., Nettleton, M. Y., & Kochan, J. P. (1993) *J. Biol. Chem. 268*, 13118−13127.

Beavil, A. J., Edmeades, R. L., Gould, H. J., & Sutton, B. J. (1992) *Proc. Natl. Acad. Sci. U.S.A. 89*, 753−757.

Beavil, A. J., Young, R. J., Sutton, B. J., & Perkins, S. J. (1995) *Biochemistry 34*, 14449−14461.

Beavil, R. L., Graber, P., Aubonney, N., Bonnefoy, J.-Y., & Gould, H. J. (1995) *Immunology 84*, 202−206.

Bebbington, C. R., Reuner, G., Thomson, S., King, D., Abrams, D., & Yarranton, G. T. (1992) *Bio/Technology 10*, 169−175.

Bettler, B., Maier, R., Rüegg, D., & Hofstetter, H. (1989) *Proc. Natl. Acad. Sci. U.S.A. 86*, 7118−7122.

Bettler, B., Texido, G., Raggini, S., Rüegg, D., & Hofstetter, H. (1992) *J. Biol. Chem. 267*, 185−191.

Cantor, C. R., & Schimmel, P. R. (1980) *Biophysical Chemistry Part III: The behaviour of biological macromolecules*, pp 874−878, W. H. Freeman and Co., New York.

Cockett, M. I., Bebbington, C. R., & Yarranton, G. T. (1990) *Bio/Technology 8*, 662−667.

Crothers, D. M., & Metzger, H. (1972) *Immunochemistry 9*, 341−357.

Cunningham, B. C., Ultsch, M., Devos, A. M., Mulkerrin, M. G., Clauser, K. R., & Wells, J. A. (1991) *Science 254*, 821−825.

Deisenhofer, J. (1981) *Biochemistry 20*, 2361−2370.

Delespesse, G., Suter, U., Mossalayi, D., Bettler, B., Sarfati, M., Hofstetter, H., Kilcherr, R., Debre, P., & Dalloul, A. (1989) *Adv. Immunol. 49*, 149−189.

Dierks, S. E., Bartlett, W. C., Edmeades, R. L., Gould, H. J., Rao, M., & Conrad, D. H. (1993) *J. Immunol. 150*, 2372−2382.

Durchschlag, H. (1986) in *Thermodynamic Data for Biochemistry and Biotechnology* (Hinz, H.-J., Ed.) pp 45−128, Springer-Verlag, Berlin.

Ghirlando, R., Keown, M. B., Mackay, G. A., Lewis, M. S., Unkeless, J. C., & Gould, H. J. (1995) *Biochemistry 34*, 13320−13327.

Gordon, J., Flores-Romo, L., Cairns, J. A., Millsum, M. J., Lane, P. J., Johnson, G. D., & MacLennan, I. C. M. (1989) *Immunol. Today 10*, 153−157.
Gordon, J., Cairns, J., Liu, J.-Y., Flores-Romo, L., Jansen, K. U., & Bonnefoy, J-Y. (1991) in *CD23: A novel multifunctional regulator of the immune system* (Gordon, J., Ed.) pp 156−168, Karger Basel.
Gustavsson, S., Hjulstrom, S., Liu, T. M., & Heyman, B. (1994) *J. Immunol. 152*, 4793−4800.
Helm, B. A., Ling, Y., Teale, C., Padlan, E. A., & Bruggemann, M. (1991) *Eur. J. Immunol. 21*, 1543−1548.
Heyman, B., Liu, T. M., & Gustavsson, S. (1993) Eur. *J. Immunol. 23*, 1739−1742.
Hoppe, H.-J., & Reid, K. B. M. (1994) *Structure 2*, 1129−1133.
Ikuta, K., Takami, M., Kim, C. W., Honjo, T., Miyoshi, T., Tagaya, Y., Kawabe, T., & Yodoi, J. (1987) *Proc. Natl. Acad. Sci. U.S.A. 84*, 819−823.
Kehry, M. R., & Yamashita, L. C. (1989) *Proc. Natl. Acad. Sci. U.S.A. 86*, 7556−7560.
Kenten, J. H., Molgaard, H. V., Houghton, M., Derbyshire, R. B., Viney, J., Bell, L. O., & Gould, H. J. (1982) *Proc. Natl. Acad. Sci. U.S.A. 79*, 6661−6665.
Keown, M. B., Ghirlando, R., Young, R. J., Beavil, A. J., Owens, R. J., Perkins, S. J., Sutton, B. J., & Gould, H. J. (1995) *Proc. Natl. Acad. Sci. U.S.A. 92*, 1841−1845.
Keown, M. B., Ghirlando, R., Mackay, G. A., & Gould, H. J. (1997) *Eur. Biophys. J.* (in press).
Laemmli, U. K. (1970) *Nature 227*, 680−685.
Melewicz, F. M., Plummer, J. M., & Spiegelberg, H. L. (1982) *J. Immunol. 129*, 563−569.
Padlan, E. A., & Davies, D. R. (1986) *Mol. Immunol. 23*, 1063−1075.
Padlan, E. A., & Helm, B. A. (1993) *Receptor 3*, 325−341.
Perkins, S. J. (1986) *Eur. J. Biochem. 157*, 169−180.
Pirron, U., Schlunck, T., Prinz, J. C., & Rieber, E. P. (1990) *Eur. J. Immunol. 20*, 1547−1551.
Provencher, S. W., & Glockner, J. (1981) *Biochemistry 20*, 33−37.
Ravetch, J. V., & Kinet, J.-P. (1991) *Annu. Rev. Immunol. 9*, 457−492.
Sarfati, M., Bettler, B., Letellier, M., Fournier, S., Rubio-Truillo, M., Hofstetter, H., & Delespesse, G. (1992) *Immunology 76*, 662−667.
Sherriff, S., Chang, C. Y. Y., & Ezekowitz, R. A. B. (1994) *Nat. Struct. Biol. 1*, 789−794.
Spiegelberg, H. L. (1984) *Adv. Immunol. 35*, 61−88.
Spolar, R. S., & Record, M. T. (1994) *Science 263*, 777−784.
Sutton, B. J., & Gould, H. J. (1993) *Nature 366*, 421−428.
Weber, G. (1975) *Adv. Protein Chem. 29*, 1−83.
Weis, W. I., & Drickamer, K. (1994) *Structure 2*, 1227−1240.
Weis, W. I., Kahn, R., Fourme, R., Drickamer, K., & Hendrickson, W. A. (1991) *Science 254*, 1608−1615.
Weis, W. I., Drickamer, K., & Hendrickson, W. A. (1992) *Nature 360*, 127−134.
Wetlaufer, D. B. (1962) *Adv. Protein Chem. 17*, 303−390.
Yokota, A., Yukawa, K., Yamamoto, A., Sugiyama, K., Suemura, M., Tashiro, Y., Kishimoto, T., & Kikutani, H. (1992) *Proc. Natl. Acad. Sci. U.S.A. 89*, 5030−5034.
Yoo, S. H., & Lewis, M. S. (1995) *Biochemistry 34*, 632−638.
Young, R. J., Owens, R. J., Mackay, G. A., Chan, C. M. W., Shi, J., Hide, M., Francis, D. M., Henry, A. J., Sutton, B. J., & Gould, H. J. (1995) *Protein Eng. 8*, 193−199.

BI961231E